Am J Nucl Med Mol Imaging 2015;5(4):379-389
www.ajnmmi.us /ISSN:2160-8407/ajnmmi0007904

Original Article

PET imaging of glioblastoma multiforme EGFR expression for therapeutic decision guidance

Eric Wehrenberg-Klee[1], Navid Redjal[2], Alicia Leece[1], N Selcan Turker[1], Pedram Heidari[1], Khalid Shah[2], Umar Mahmood[1]

[1]Athinoula A. Martinos Center for Biomedical Imaging, Massachusetts General Hospital, Harvard Medical School, Boston, MA; [2]Molecular Neurotherapy and Imaging Laboratory, Department of Radiology and Neurology, Massachusetts General Hospital, Harvard Medical School, Boston, MA

Received March 12, 2015; Accepted April 6, 2015; Epub June 15, 2015; Published July 1, 2015

Abstract: After initial therapy and total resection of glioblastoma multiforme (GBM), 80-90% of recurrences occur at the surgical margins. Insufficient sensitivity and specificity of current imaging techniques based on non-specific vascular imaging agents lead to delay in diagnosis of residual and/or recurrent disease. A tumor-specific imaging agent for GBM may improve detection of small residual disease in the post-operative period, and improve ability to distinguish tumor recurrence from its imaging mimics that can delay diagnosis. To this end, we developed an EGFR-targeted PET probe and assessed its ability to image EGFR WT (U87) and EGFRvIII (Gli36vIII) expressing GBMs in both murine intra-cranial xenografts and in a surgical-resection model. The developed imaging probe, ^{64}Cu-DOTA-cetuximab-F(ab´)$_2$, binds with a K_d of 11.2 nM to EGFR expressing GBM. ^{64}Cu-DOTA-cetuximab-F(ab´)$_2$ specifically localized to intra-cranial tumor with a significant difference in SUVmean between tumor and contralateral brain for both Gli36vIII and U87 tumors (P<0.01 for both comparisons), with mean TBR of 22.5±0.7 for Gli36vIII tumors and 28.9±2.1 for U87 tumors (TBR±SEM). Tracer uptake by tumor was significantly inhibited by pre-injection with cetuximab (P<0.01 for both), with SUVmean reduced by 68% and 58% for Gli36vIII and U87 tumors, respectively. Surgical resection model PET-CT imaging demonstrates residual tumor and low nonspecific uptake in the resection site. We conclude that ^{64}Cu-DOTA-cetuximab-F(ab´)$_2$ binds specifically to intracranial EGFR WT and EGFRvIII expressing GBM, demonstrates excellent TBR, and specifically images small residual tumor in a surgical model, suggesting future clinical utility in identifying true tumor recurrence.

Keywords: Glioblastoma, imaging, PET, EGFR, EGFRvIII, recurrence, residual disease, surgical margin

Introduction

Initial treatment for glioblastoma multiforme (GBM) is surgery followed by adjuvant treatment with temozolomide and radiation [1]. Following initial therapy and complete resection as evaluated by MRI, 80-90% of tumor recurrences occur at the surgical margin [2-4]. Limitations of current imaging techniques may contribute to delayed detection of residual and recurrent disease, as contrast-enhanced MRI is limited in its ability to distinguish small residual tumor from the non-specific contrast-enhancement of post-operative inflammation, as well the imaging mimics of pseudoprogression and radiation necrosis [5-7]. Significant effort has gone into the development of more sensitive intra-operative and post-operative imaging techniques to distinguish small foci of residual and recurrent tumor. Intra-operatively, the utility of fluorescent dyes such as 5-aminolevulinic acid has been investigated, with some success at distinguishing residual tumor in comparison to MRI [8]. Post-operatively, multiple PET and MRI imaging agents and techniques have been employed in an attempt to improve the sensitivity for residual and recurrent tumor detection, and also increase ability to distinguish true recurrence from pseudoprogression. MRI techniques have focused on the use of relative cerebral blood volume (rCBV), with higher rCBV values being associated with the tumor neovascularization [9-11]. PET techniques have included the use of ^{11}C-methionine [12]. All of these strategies are based on indirect measures of tumor growth, and have demonstrated limited clinical diagnostic utility to date.

An imaging agent that directly and specifically highlights GBM tumor cells may increase the ability to recognize residual and recurrent tumor in the surgical bed as well as distinguish tumor progression from its imaging mimics, with potential for improving post-operative outcomes. EGFR is highly over-expressed on 40-60% of GBMs, and EGFR expression status for individual patients is known after initial resection as part of standard-of-care pathological assessment [13-15]. We hypothesized that a specific EGFR-targeted imaging agent could image EGFR-expressing GBMs and, in the future, provide a novel mechanism for recognizing residual tumor in those GBM patients with confirmed baseline tumoral EGFR over-expression.

We developed and pre-clinically tested a novel PET probe, ^{64}Cu-DOTA-cetuximab F(ab´)$_2$, for direct imaging of GBMs expressing either EGFR wild-type or the EGFRvIII mutant, a common variant to which cetuximab also binds with high affinity [16]. Our studies demonstrate that our imaging agent can specifically image EGFR wild-type and EGFRvIII-expressing intracranial GBMs. We also successfully image EGFR expressing GBMs in a surgical resection model that suggests future clinical applicability. Our imaging approach allows for direct GBM tumor cell imaging, which could improve the detection of residual and/or recurrent tumor in the surgical bed over current imaging technology.

Methods

Cell culture

U87, a GBM cell line that expresses wild-type EGFR, was used for cell binding studies. Animal studies were conducted with both U87 and Gli36vIII, a GBM cell line that has been engineered to express EGFRvIII [17]. Both of these cell lines have also been engineered to express either GFP-Fluc fusion protein (LV-GFP-Fluc) (U87) or mCherry-Fluc fusion protein (LV-mCherry-Fluc) (Gli36vIII) [18, 19]. Cells were cultured in DMEM medium (ATCC), supplemented by 10% (v/v) FBS, 100 U/mL penicillin, and 100 μg/mL streptomycin. Cultures were maintained in a humidified incubator at 37°C, 5% CO_2. Subculturing was performed employing a 0.25% trypsin-0.1% EDTA solution.

Preparation of DOTA-cetuximab-F(ab´)$_2$

FragIt Kits (Genovis, Lund, Sweden) were used per the manufacturer's protocol with 1 mg of cetuximab (ImClone, New York, NY), a commercially approved monoclonal antibody with high specificity for the external domain of EGFR [20], to generate and isolate F(ab´)$_2$ fragments [21]. Generation and isolation of F(ab´)$_2$ fragments was confirmed with gel-electrophoresis, and final concentration was determined by UV absorbance at 280 nm. For DOTA conjugation to F(ab´)$_2$ 1.5 mg of cetuximab-F(ab´)$_2$ were added to SCN-DOTA (Macrocyclics, Dallas, TX) in 500 μL anhydrous-DMSO in a 1:10 molar ratio and incubated over night at 4°C. Purification of conjugated DOTA-cetuximab F(ab´)$_2$ was achieved by addition of 12 ml of 0.1 M ammonium acetate (pH 6) to the reaction solution and centrifugation at 4000 g × 15 min on a 10 κD MW Amicon-4 filtration devices (EMD Millipore, Billerica, MA), repeated six times [22]. The number of DOTA chelators per cetuximab F(ab´)$_2$ was determined by labeling a 10 μL aliquot of the unpurified conjugation reaction with ^{67}Ga, and then determining the proportion of ^{67}Ga-DOTA-cetuximab F(ab´)$_2$ vs. free ^{67}Ga-DOTA by ITLC with silica gel solid phase and 100 mM sodium citrate, pH 5 mobile phase, with Rf of 0 and 1, respectively, and then multiplying this fraction by the molar ratio of the conjugation reaction [23].

^{64}Cu and ^{67}Ga labeling of DOTA-cetuximab-F(ab´)$_2$

Approximately 5 mCi of $^{64}CuCl_2$ (University of Wisconsin, Madison, Wisconsin) was diluted in 400 μL of 0.25 M ammonium acetate buffer at pH 5.5, to which 6 μg of DOTA-cetuximab-F(ab´)$_2$ was added for a final reaction volume of 500 μL. The reaction was incubated at 40°C for 90 min, and then purified through centrifugation at 3500 RPM for 10 minutes ×4 using Amicon-4 filters and sterile saline as the mobile phase. Labeled compound purity was determined on a gamma counter (Wizard 2480, Perkin Elmer, MA) after size-exclusion chromatography purification (PD-10, GE Healthcare Bio-Sciences AB, Björkgatan, Uppsala, Sweden). $^{67}GaCl_3$ was obtained from Nordion (Ontario, Ottawa, CAN). Labeling with ^{67}Ga was chosen for *in vitro* experiments due to improved ease of use, and proceeded under similar conditions as to ^{64}Cu, with reaction pH held between 4-4.5.

Direct radioligand binding

Binding affinity of ^{67}Ga-DOTA-cetuximab-F(ab´)$_2$ was determined by direct (saturation) radioligand binding assays in triplicate using a fixed

concentration of cetuximab and increasing concentration of ^{67}Ga-DOTA-cetuximab-F(ab´)$_2$ on U87 cells. Increasing concentrations (0 to 100 nmol/L) of ^{67}Ga-DOTA-cetuximab-F(ab´)$_2$ were incubated with 1×10^5 cells in 24-well plates at 4°C for 3 h. Unbound radioactivity was removed and the dishes were rinsed three times with ice-cold PBS and detached with trypsin. The number of cells in each well was counted using an automated cell counter (Countess®, Invitrogen, Carlsbad, CA) and the total cell-bound radioactivity (TB) was measured in a gamma counter (Wizard 2480, Perkin Elmer, MA). The assay was repeated in the presence of 16 μmol/L of unlabeled cetuximab to measure non-specific binding (NSB) at 4°C for 2 h. Specific binding (SB) was calculated by subtracting NSB from TB and was plotted vs. the concentration of ^{67}Ga-DOTA-cetuximab-F(ab´)$_2$ added. The resulting curve was fitted by non-linear regression to a one-site receptor-binding model by Prism Ver. 4.0 software (GraphPad, San Diego, CA). The dissociation constant (K_D) and maximum number of receptors per cell (Bmax) was calculated.

Intracranial cell implantation and bioluminescence imaging in vivo

All experimental protocols were approved by the Animal Care and Use Committees at Massachusetts General Hospital. Orthotopic intracranial tumor models were developed first by harvesting U87 (4×10^5) and Gli36vIII (2×10^5) cells at 80% confluence, and implanting them stereotactically into the right frontal lobe of adult nude mice brains (n=10 for each cell line), 2 mm lateral to the bregma and 0.5 mm from the dura. Two weeks after implantation, mice were injected intra-peritoneally with 4.5 mg of D-luciferin, and imaged on a Carestream multi-spectral imaging system (Rochester, NY, USA) to confirm tumor growth through bioluminescence imaging.

In vivo imaging studies

Two weeks after intracranial implantation, both U87 and Gli36vIII-implanted mice were randomized to intravenous tail-vein injection with 200 μCi ^{64}Cu-DOTA-cetuximab-F(ab´)$_2$ alone, or blocking with intravenous tail-vein injection of 2.5 mg of cetuximab followed by injection of 200 μCi ^{64}Cu-DOTA-cetuximab-F(ab´)$_2$ twenty-four hours later (n=5 for each group). Twenty-four hours following injection with ^{64}Cu-DOTA-cetuximab-F(ab´)$_2$, mice underwent static PET-CT imaging using a Sedecal SuperArgus PET/CT (Madrid, Spain). CT images were obtained at 150 mA and 45 kV for a standard resolution of 200 μM, 360°, and 16 shots with 1 bed position. PET images were obtained for 15 min in 2 bed positions. Images were reconstructed using 3D-OSEM (4 iterations, 16 subsets) and were corrected for scatter and randoms. The mean standard uptake value (SUVmean) for each tumor was calculated in a 3D region of interest auto-drawn around the tumor using a 30% isocontour threshold. SUVmean in the contralateral brain was calculated by selecting a 1 mm circular region of interest in the contralateral frontal lobe over three contiguous slices. Images were post-processed using VivoQuant (InviCRO, Boston, MA).

Fluorescence-guided resection model and PET imaging

Nude mice were used for the intracranial xenograft GBM model. U87-GFP-Fluc were harvested at 80% confluency and implanted stereotactically (4×10^5 cells) as above. Tumor resection protocol has been previously described in detail [24]. In brief, on the day of resection, tumor growth was confirmed with bioluminescence imaging (BLI). Following immobilization on a stereotactic frame mice were placed under an Olympus SZ10x microscope (Olympus, Center Valley, PA). Intraoperative microscopic white light and GFP images were captured throughout the procedure using a DP-72 camera and CellSens software (Olympus). After incision of the skin, skull, and dura, the U87-GFP-Fluc tumor was either completely or partially surgically excised using a combination of surgical dissection and aspiration. Following tumor removal, the resulting resection cavity was copiously irrigated and the skin closed with 7-0 Vicryl suture (JAJ, New Brunswick, NJ). Ten days following surgery, bioluminescence imaging was used to confirm absence of tumor or residual tumor in complete and partial resection mice, respectively. Both complete resection and partial resection mice were then injected with ~200 μCi ^{64}Cu-DOTA-cetuximab-F(ab´)$_2$, and PET-CT images obtained twenty-four hours later as described above.

Statistical analysis

Statistical analysis was performed using Graphpad Prism Version 4. Two-way paired t-test was used to compare SUVmean of tum-

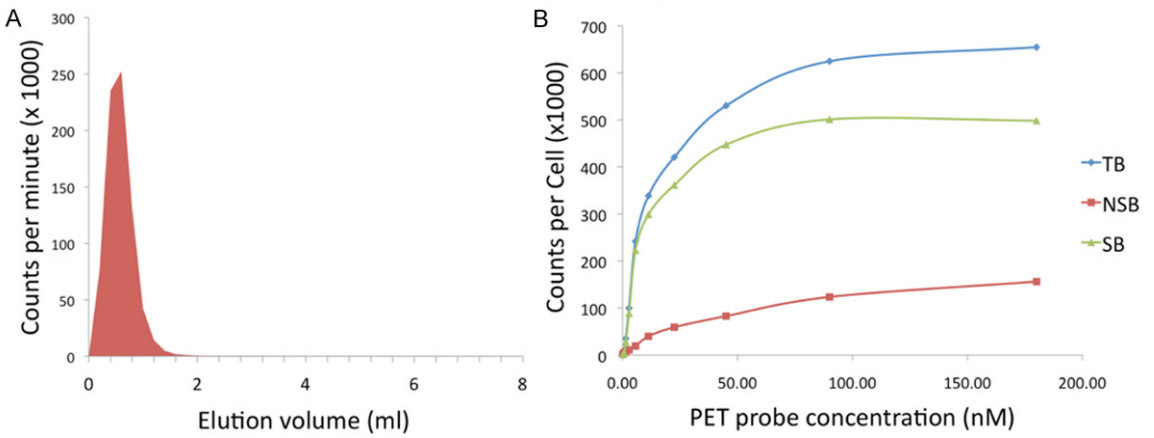

Figure 1. Generation and characterization of the developed PET probe. A. Size-exclusion chromatography demonstrates DOTA-cetuximab-F(ab´)$_2$ is labeled with ^{64}Cu with >95% radiochemical purity. B. The developed PET imaging agent has a high affinity for the target, evidenced by a Kd of 11.2 nM for EGFR assessed using U87 cells.

ors to contra-lateral normal brain. Two-way unpaired t-test was used to compare SUVmean of blocked vs. non-blocked in vivo tumors. All PET uptake values are reported as SUVmean ± standard error of the mean. A $P<0.05$ was considered statistically significant.

Immunohistochemistry

Tumor bearing mice were euthanized and perfused with formalin and PBS. Brain tissue was fixed in 30% sucrose in PBS, frozen, and 10 micron slices were sectioned. Immunohistochemistry was performed on brain sections using anti-EGF Receptor XP® Rabbit monoclonal antibody (Cell Signaling, Danvers, MA) primary antibody for U87 sections and anti-EGFRvIII rabbit polyclonal antibody (Bioss, Woburn, MA) for Gli36vIII sections. After primary antibody incubation and washing, sections were incubated with anti-rabbit IgG-HRP. Sections were then developed with DAB (Dako, Carpinteria, CA), and then counterstained with hematoxylin. White-light visualization of staining, as well as GFP and mCherry expression, was visualized by confocal microscopy using an Olympus IX51 upright microscope. Image processing was performed using Image J (NIH, Bethesda, MD).

Results

Imaging agent development

Cetuximab-F(ab´)$_2$ was generated with high-specificity by digestion of the anti-EGFR antibody cetuximab using the Fragit Kit followed by incubation on a Protein A column to remove Fc portions. DOTA, a metal chelator specific for 2+ and 3+ cations, was conjugated to cetuximab-F(ab´)$_2$ through incubation with DOTA-SCN, with an average of 1.4 DOTA equivalents bound to each molecule of cetuximab-F(ab´)$_2$. DOTA-cetuximab-F(ab´)$_2$ was labeled with the gamma-emitting radiometal ^{67}Ga for determination of K_d with U87 cells *in vitro*, and labeled with the positron-emitting radiometal ^{64}Cu for *in vivo* studies. Radiolabelling proceeded with radiochemical purity of >95%, as assessed by size-exclusion chromatography (**Figure 1A**).

EGFR binding affinity

Using a saturation radio-ligand binding assay we demonstrated that ^{67}Ga-DOTA-cetuximab-F(ab´)$_2$ binds specifically to EGFR expressed on the surface of U87 cells (**Figure 1B**). The K_d value for ^{67}Ga-DOTA-cetuximab-F(ab´)$_2$ binding to EGFR was 11.2 nM.

In vitro imaging

Confocal microscopy of resected GFP-expressing U87 gliomas and mCherry-expressing Gli36vIII gliomas confirmed cell-type. Immunohistochemistry with antibodies specific for EGFR WT and EGFRvIII for U87 and Gli36vIII cells, respectively, confirmed tumoral EGFR expression, and lack of expression in adjacent normal brain parenchyma (**Figure 2**).

In vivo imaging of tumor detection

PET-CT imaging of intracranial U87 tumors 24 hours after injection of ^{64}Cu-DOTA-cetuximab-

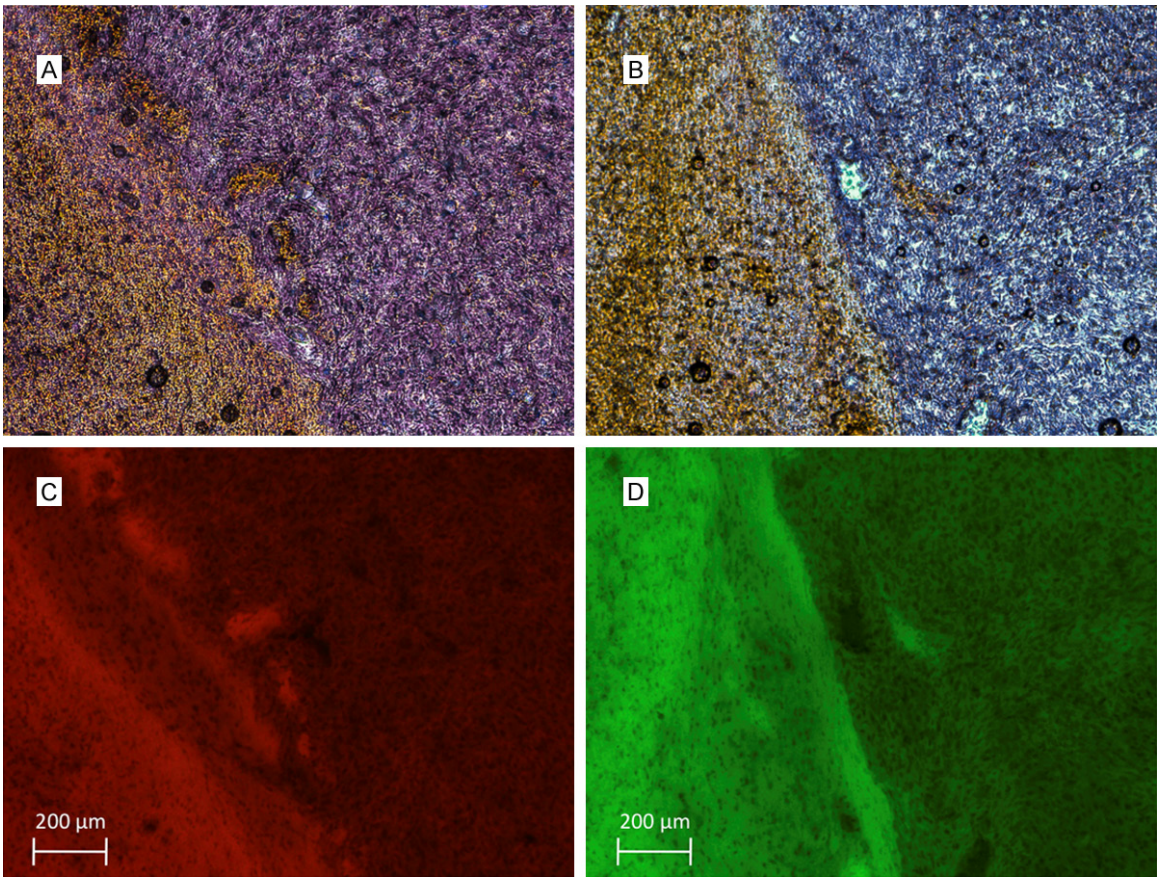

Figure 2. EGFR immunohistochemistry demonstrates EGFRvIII and EGFR wild-type expression on (A) Gli36vIII and (B) U87 cells. Fluorescent micrographs demonstrate mCherry expression of (C) Gli36vIII and GFP expression of (D) U87 cells that correlate with areas of EGFR expression.

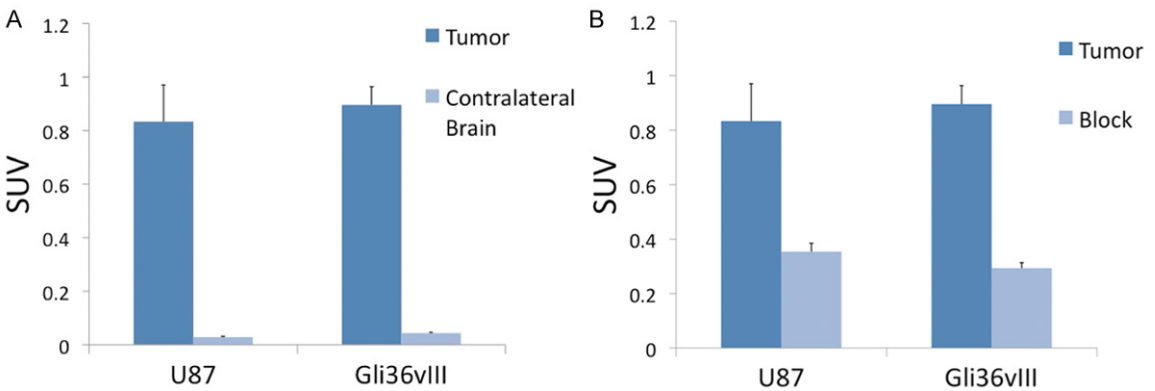

Figure 3. In vivo assessment of EGFR targeted PET probe. Comparison of SUVmean of tumor versus contralateral brain 24 hours after injection of ^{64}Cu-DOTA-cetuximab-F(ab´)$_2$ demonstrates TBR of 27.7 for U87 tumors and 22.5 for Gli36vIII, P<0.01 for both tumor types compared to contralateral normal brain (A). Mice bearing intracranial U87 or Gli36vIII tumors were injected were intravenously injected with 2.5 mg cetuximab 24 h prior to tracer injection. Blocking resulted in a 58% and 68% reduction in SUV for U87 and Gli36vIII tumors, respectively, P<0.05 for both tumor types (B).

F(ab´)$_2$ demonstrated a SUVmean of 0.83 (±0.13) compared to SUVmean of 0.03 (±0.003) in contra-lateral brain (P<0.01), with a tumor-to-background ratio (TBR) of 28.9 (±2.1) (**Figure**

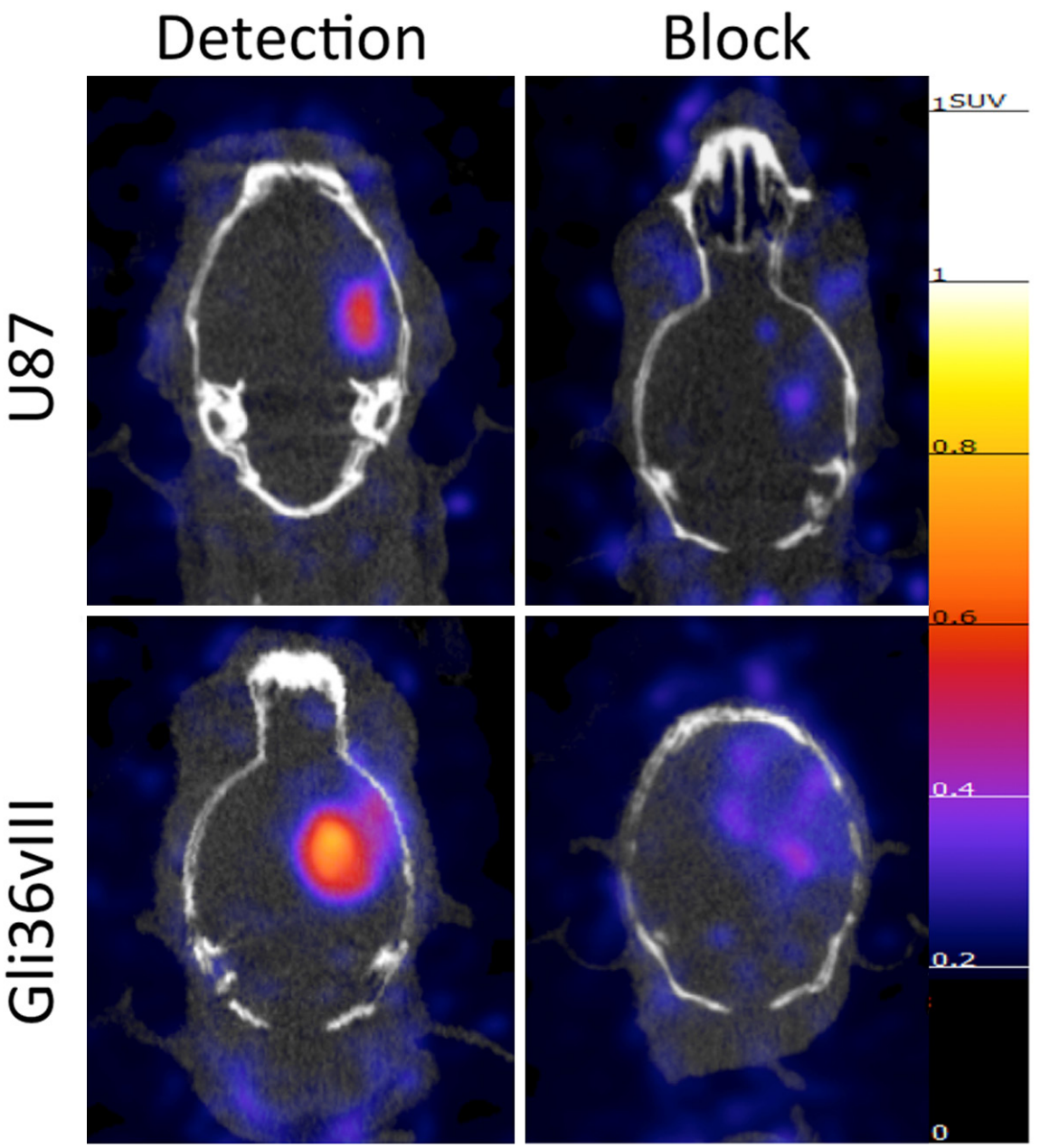

Figure 4. Representative PET-CT images of the EGFR targeted probe with and without target block. ^{64}Cu-DOTA-cetuximab-F(ab´)$_2$ was injected 24 hours before imaging of mice bearing intracranial U87 or Gli36vIII tumors. Imaging demonstrates high tumor uptake in both U87 (EGFR wild type) and Gli36vIII (EGFRvIII mutant) tumors (left panels), which is abrogated with pretreatment with cetuximab 24 h prior to tracer injection tracer (right panels). All PET images normalized to 1.25 SUV.

3). PET-CT imaging of intracranial Gli36vIII tumors 24 hours after injection of 200 μCi ^{64}Cu-DOTA-cetuximab-F(ab´)$_2$ demonstrated a SUVmean of 0.90 (±0.07) compared to a SUVmean of 0.04 (±0.003) in contra-lateral brain (P<0.01), resulting in a TBR of 22.5 (±0.7) (**Figure 3A**).

In vivo imaging with target blocking

PET-CT imaging of intracranial U87 tumors 48 hours after tail-vein injection of cetuximab demonstrated a SUVmean of 0.35 (±0.03), a decrease of 58% relative to unblocked tumor SUVmean (P<0.05). PET-CT imaging of intracra-

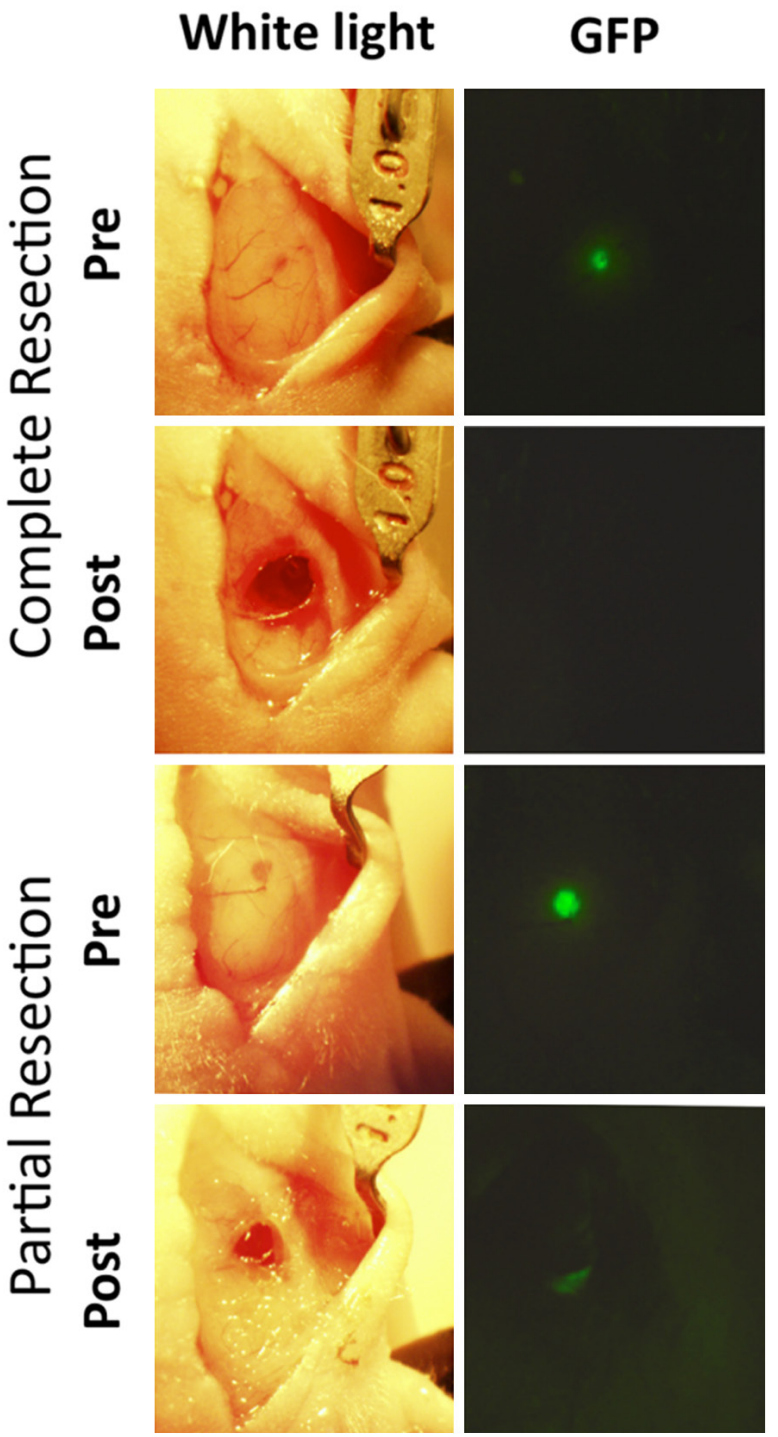

Figure 5. Complete and partial resection of intracranial GBM. White-light (left panels) and GFP (right panels) pre and post complete or partial resection of intracranial U87 tumors demonstrate surgical technique and visual confirmation of technical success with both complete and partial resection.

nial Gli36vIII tumors 48 hours after tail-vein injection of cetuximab demonstrated a tumor SUVmean of 0.29 (±0.02), a decrease of 68% relative to non-block tumor SUVmean (P<0.01) (**Figure 3B**). Representative axial PET-CT images of intracranial U87 and Gli36vIII (**Figure 4**, left panel) tumors clearly demonstrate tumor distinct from brain parenchyma. Representative images after blocking with cetuximab demonstrate reduction in tumor SUV post-blocking (**Figure 4**, right panel).

In vivo imaging of glioblastoma multiforme resection model

Orthotopically implanted intracranial U87 tumors were either completely or partially resected, with GFP-imaging demonstrating complete removal of tumor in complete resection mouse, and residual tumor in partial resection mouse (**Figure 5**). BLI ten days post-resection confirmed absence of tumor in complete resection mouse and presence of tumor in partial resection mouse model. PET-CT images of mice obtained 24 h after injection with 200 μCi EGFR PET Probe demonstrated tracer uptake in partial-resection tumor, and no tracer uptake above background in surgical cavity of complete resection model (**Figure 6**).

Discussion

Current imaging techniques for GBM rely on non-specific contrast-enhancement or indirect measures of tumor growth that are insufficiently sensitive and do not provide the necessary diagnostic certitude to guide treatment. A PET imaging agent that specifically binds tumor may, when used in conjunction with contrast enhanced MRI, improve post-operative

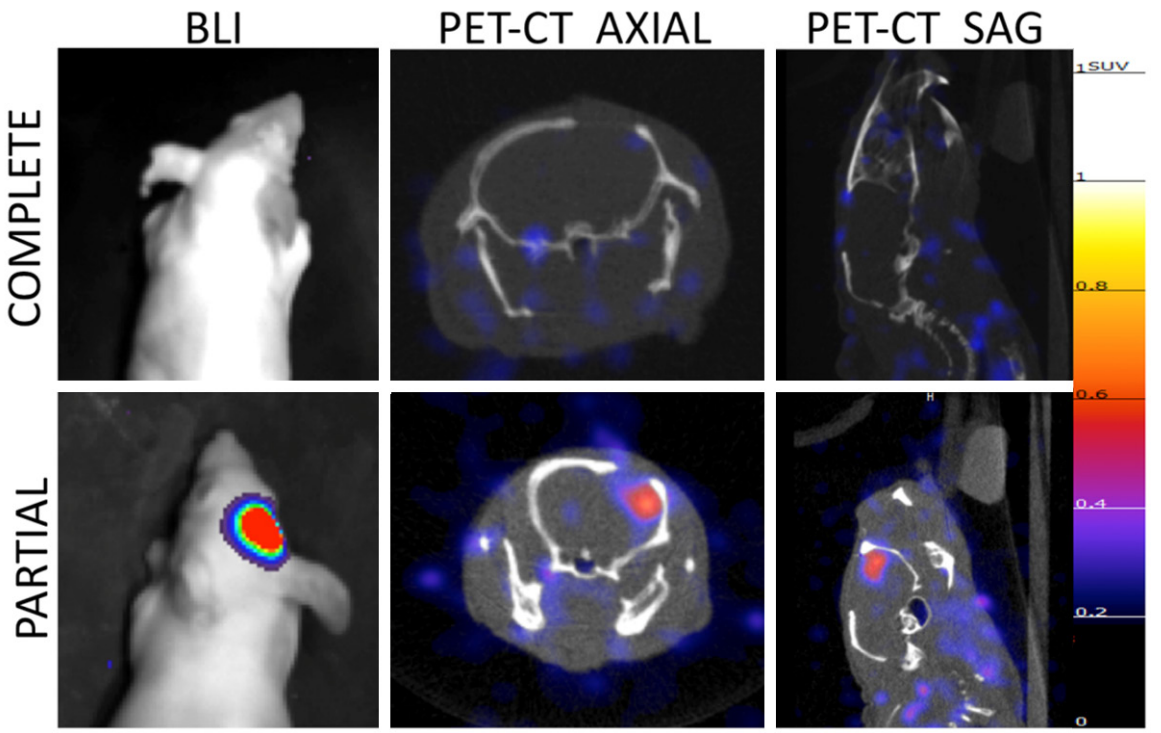

Figure 6. PET-CT and bioluminescence imaging of resection model mice post-surgery. 10 days post surgery both complete (upper panel) and partial resection (lower panel) mice were imaged with bioluminescence imaging demonstrating absence of tumor in complete resection model and residual tumor in partial resection model. PET-CT imaging of resection model mice demonstrates no tracer uptake above background in complete resection mouse and residual tumor in partial resection mouse. All PET images normalized to 1.25 SUV.

discrimination of residual tumor, and be able to distinguish true progression from its imaging mimics, potentially reducing recurrence rates as well as sparing patients unnecessary diagnostic interventions.

We have developed an EGFR-specific antibody-based PET imaging agent, and demonstrated in an intracranial mouse model that we can specifically image EGFR wild-type and EGFRvIII expressing GBMs. In both of the GBM models we investigated, we demonstrate excellent tumor to background SUV ratios of 28.9 and 22.5 for U87 and Gli36vIII, respectively. We note that ex-vivo activity measurements of tumor and contralateral brain that could have corroborated our SUV measurement were not performed. These measured tumors to background ratios provide more than sufficient contrast for ready clinical interpretation. Our imaging agent takes advantage of the fact that while EGFR is overexpressed on many GBMS, EGFR is not highly expressed in most normal brain tissue [25, 26]. The high-degree of disparity in EGFR expression between normal brain tissue and malignant tissue allows for generation of high tumor to background ratios. With a reduced molecular weight relative to whole antibodies that allows for more rapid systemic clearance, our imaging agent has a favorable pharmacokinetic profile for human translation. Finally, as the developed imaging agent is based on a clinically approved therapeutic agent, with the injected dose for imaging less than 1/1000 of the clinical dose, a high safety profile is expected for future clinical translation.

We demonstrate that ^{64}Cu-DOTA-cetuximab-F(ab´)$_2$ binds to EGFR-expressing GBM, with tracer uptake reduced by approximately two thirds with pre-injection of cetuximab 24 hours prior to tracer injection. The non-specific activity that remains in the region of the tumor after blocking with whole antibody may be secondary to a well-documented phenomenon of enhanced permeability and retention (EPR), whereby macromolecules preferentially accumulate in tumor tissue in part due to the increased permeability of the tumor neovascu-

lature [27]. We further note that determination of non-specific probe binding may have been improved with the used of an EGFR-negative tumor line rather than blocking studies, by eliminating the possibility of on-target binding and without raising the question of vascular normalization after treatment with angiogenic inhibitors. To our knowledge there is no evidence of significant vascular normalization in glioblastoma models secondary to cetuximab over the relevant time frame (24-48 h), but other pure angiogenic inhibitors have demonstrated early tumor vasculature normalization as early as 48 h post-treatment, and those same effects could be active in our model [28]. Given the high degree of specific uptake relative to non-specific uptake, utilization of thresholding techniques commonly applied throughout imaging interpretation should be sufficient to distinguish EGFR-expressing tumor from non-specific permeability effects. By means of comparison, in studies of the recently FDA approved beta-amyloid imaging agent florbetapir, a SUV ratio between cortex and cerebellum of >1.1 was determined the appropriate threshold for a positive study [29].

In a surgical resection model of GBM we demonstrate both that our probe can identify residual tumor after partial resection and that there is no uptake of tracer above background in the remainder of the surgical bed. These results suggest the utility of the developed agent in a surgical setting, where it could be used shortly after surgery to detect residual unresected tumor with greater sensitivity and specificity than current imaging techniques, and could potentially help to reduce the high rate of recurrence within the surgical bed. For imaging monitoring of patients over the medium-term, it has been shown in one retrospective study of EGFRvIII-expressing GBM that EGFRvIII mRNA levels can decrease by as much as 50% in recurrent tumors relative to initial resection [30]. The impact of this reduction in EGFRvIII mRNA on the ability of the designed EGFR PET probe to detect recurrent EGFRvIII expressing tumors would need to be further evaluated in future studies.

Due to the lack of pseudoprogression mouse models, we are unable to specifically demonstrate the utility of our imaging agent in distinguishing tumor recurrence from pseudoprogression. However, as our imaging agent specifically binds EGFR-expressing tumor, it may have a role in distinguishing tumor recurrence from its non-specific imaging mimics that are secondary to blood-brain barrier breakdown. This could have significant clinical benefit, as it is believed that up to 64% of patients with apparent progression of disease on imaging have pseudoprogression only [31]. Currently, the inability to accurately and consistently distinguish between GBM true progression and pseudoprogression causes confusion in clinical decision-making, which leads to marked delays in treatment, and frequently necessitates repeat brain biopsy with its attendant risks.

Finally, in patients whose tumors do not significantly over-express EGFR, other surface receptors such as c-MET, which is over-expressed in approximately 30% of GBMs, could represent targets for alternative imaging agents [32]. With the development of only a few receptor specific imaging agents, used singly for individual patients, the vast majority of GBMs could potentially be imaged after front-line therapy with sufficient diagnostic accuracy to guide subsequent treatment.

Acknowledgements

This research was supported in part by U01CA084301, P50CA127003 and R01CA-173077.

Disclosure of conflict of interest

None.

Address correspondence to: Dr. Umar Mahmood, Athinoula A. Martinos Center for Biomedical Imaging, Department of Radiology, Massachusetts General Hospital, Boston, MA. Tel: 617-726-6477; E-mail: umahmood@mgh.harvard.edu

References

[1] Stupp R, Mason WP, van den Bent MJ, Weller M, Fisher B, Taphoorn MJ, Belanger K, Brandes AA, Marosi C, Bogdahn U, Curschmann J, Janzer RC, Ludwin SK, Gorlia T, Allgeier A, Lacombe D, Cairncross JG, Eisenhauer E and Mirimanoff RO. Radiotherapy plus concomitant and adjuvant temozolomide for glioblastoma. N Engl J Med 2005; 352: 987-996.

[2] Petrecca K, Guiot MC, Panet-Raymond V and Souhami L. Failure pattern following complete resection plus radiotherapy and temozolomide is at the resection margin in patients with glioblastoma. J Neurooncol 2013; 111: 19-23.

[3] Chamberlain MC. Radiographic patterns of relapse in glioblastoma. J Neurooncol 2011; 101: 319-323.
[4] McDonald MW, Shu HK, Curran WJ Jr and Crocker IR. Pattern of failure after limited margin radiotherapy and temozolomide for glioblastoma. Int J Radiat Oncol Biol Phys 2011; 79: 130-136.
[5] Gerstner ER, McNamara MB, Norden AD, Lafrankie D and Wen PY. Effect of adding temozolomide to radiation therapy on the incidence of pseudo-progression. J Neurooncol 2009; 94: 97-101.
[6] Taal W, Brandsma D, de Bruin HG, Bromberg JE, Swaak-Kragten AT, Smitt PA, van Es CA and van den Bent MJ. Incidence of early pseudoprogression in a cohort of malignant glioma patients treated with chemoirradiation with temozolomide. Cancer 2008; 113: 405-410.
[7] Brandsma D, Stalpers L, Taal W, Sminia P and van den Bent MJ. Clinical features, mechanisms, and management of pseudoprogression in malignant gliomas. Lancet Oncol 2008; 9: 453-461.
[8] Coburger J, Engelke J, Scheuerle A, Thal DR, Hlavac M, Wirtz CR and Konig R. Tumor detection with 5-aminolevulinic acid fluorescence and Gd-DTPA-enhanced intraoperative MRI at the border of contrast-enhancing lesions: a prospective study based on histopathological assessment. Neurosurg Focus 2014; 36: E3.
[9] Gahramanov S, Muldoon LL, Varallyay CG, Li X, Kraemer DF, Fu R, Hamilton BE, Rooney WD and Neuwelt EA. Pseudoprogression of glioblastoma after chemo- and radiation therapy: diagnosis by using dynamic susceptibility-weighted contrast-enhanced perfusion MR imaging with ferumoxytol versus gadoteridol and correlation with survival. Radiology 2013; 266: 842-852.
[10] Hu LS, Baxter LC, Smith KA, Feuerstein BG, Karis JP, Eschbacher JM, Coons SW, Nakaji P, Yeh RF, Debbins J and Heiserman JE. Relative cerebral blood volume values to differentiate high-grade glioma recurrence from posttreatment radiation effect: direct correlation between image-guided tissue histopathology and localized dynamic susceptibility-weighted contrast-enhanced perfusion MR imaging measurements. AJNR Am J Neuroradiol 2009; 30: 552-558.
[11] Barajas RF Jr, Chang JS, Segal MR, Parsa AT, McDermott MW, Berger MS and Cha S. Differentiation of recurrent glioblastoma multiforme from radiation necrosis after external beam radiation therapy with dynamic susceptibility-weighted contrast-enhanced perfusion MR imaging. Radiology 2009; 253: 486-496.
[12] Terakawa Y, Tsuyuguchi N, Iwai Y, Yamanaka K, Higashiyama S, Takami T and Ohata K. Diagnostic accuracy of 11C-methionine PET for differentiation of recurrent brain tumors from radiation necrosis after radiotherapy. J Nucl Med 2008; 49: 694-699.
[13] Ohgaki H and Kleihues P. Genetic pathways to primary and secondary glioblastoma. Am J Pathol 2007; 170: 1445-1453.
[14] Shinojima N, Tada K, Shiraishi S, Kamiryo T, Kochi M, Nakamura H, Makino K, Saya H, Hirano H, Kuratsu J, Oka K, Ishimaru Y and Ushio Y. Prognostic value of epidermal growth factor receptor in patients with glioblastoma multiforme. Cancer Res 2003; 63: 6962-6970.
[15] Libermann TA, Nusbaum HR, Razon N, Kris R, Lax I, Soreq H, Whittle N, Waterfield MD, Ullrich A and Schlessinger J. Amplification, enhanced expression and possible rearrangement of EGF receptor gene in primary human brain tumours of glial origin. Nature 1985; 313: 144-147.
[16] Patel D, Lahiji A, Patel S, Franklin M, Jimenez X, Hicklin DJ and Kang X. Monoclonal antibody cetuximab binds to and down-regulates constitutively activated epidermal growth factor receptor vIII on the cell surface. Anticancer Res 2007; 27: 3355-3366.
[17] Bagci-Onder T, Wakimoto H, Anderegg M, Cameron C and Shah K. A dual PI3K/mTOR inhibitor, PI-103, cooperates with stem cell-delivered TRAIL in experimental glioma models. Cancer Res 2011; 71: 154-163.
[18] Shah K, Hingtgen S, Kasmieh R, Figueiredo JL, Garcia-Garcia E, Martinez-Serrano A, Breakefield X and Weissleder R. Bimodal viral vectors and in vivo imaging reveal the fate of human neural stem cells in experimental glioma model. J Neurosci 2008; 28: 4406-4413.
[19] Martinez-Quintanilla J, Bhere D, Heidari P, He D, Mahmood U and Shah K. Therapeutic efficacy and fate of bimodal engineered stem cells in malignant brain tumors. Stem Cells 2013; 31: 1706-1714.
[20] Fan Z, Masui H, Altas I and Mendelsohn J. Blockade of epidermal growth factor receptor function by bivalent and monovalent fragments of 225 anti-epidermal growth factor receptor monoclonal antibodies. Cancer Res 1993; 53: 4322-4328.
[21] von Pawel-Rammingen U, Johansson BP and Bjorck L. IdeS, a novel streptococcal cysteine proteinase with unique specificity for immunoglobulin G. EMBO J 2002; 21: 1607-1615.
[22] Chan C, Scollard DA, McLarty K, Smith S and Reilly RM. A comparison of 111In- or 64Cu-DOTA-trastuzumab Fab fragments for imaging subcutaneous HER2-positive tumor xenografts in athymic mice using microSPECT/CT or microPET/CT. EJNMMI Res 2011; 1: 15.

[23] Reilly R. Monoclonal antibody and peptide-targeted radiotherapy of cancer. Hoboken, N.J.: Wiley; 2010.
[24] Hingtgen S, Figueiredo JL, Farrar C, Duebgen M, Martinez-Quintanilla J, Bhere D and Shah K. Real-time multi-modality imaging of glioblastoma tumor resection and recurrence. J Neurooncol 2013; 111: 153-161.
[25] Werner MH, Nanney LB, Stoscheck CM and King LE. Localization of immunoreactive epidermal growth factor receptors in human nervous system. J Histochem Cytochem 1988; 36: 81-86.
[26] Fallon JH, Seroogy KB, Loughlin SE, Morrison RS, Bradshaw RA, Knaver DJ and Cunningham DD. Epidermal growth factor immunoreactive material in the central nervous system: location and development. Science 1984; 224: 1107-1109.
[27] Matsumura Y and Maeda H. A new concept for macromolecular therapeutics in cancer chemotherapy: mechanism of tumoritropic accumulation of proteins and the antitumor agent smancs. Cancer Res 1986; 46: 6387-6392.
[28] Winkler F, Kozin SV, Tong RT, Chae SS, Booth MF, Garkavtsev I, Xu L, Hicklin DJ, Fukumura D, di Tomaso E, Munn LL and Jain RK. Kinetics of vascular normalization by VEGFR2 blockade governs brain tumor response to radiation: role of oxygenation, angiopoietin-1, and matrix metalloproteinases. Cancer Cell 2004; 6: 553-563.
[29] Clark CM, Pontecorvo MJ, Beach TG, Bedell BJ, Coleman RE, Doraiswamy PM, Fleisher AS, Reiman EM, Sabbagh MN, Sadowsky CH, Schneider JA, Arora A, Carpenter AP, Flitter ML, Joshi AD, Krautkramer MJ, Lu M, Mintun MA, Skovronsky DM; AV-45-A16 Study Group. Cerebral PET with florbetapir compared with neuropathology at autopsy for detection of neuritic amyloid-beta plaques: a prospective cohort study. Lancet Neurol 2012; 11: 669-678.
[30] Montano N, Cenci T, Martini M, D'Alessandris QG, Pelacchi F, Ricci-Vitiani L, Maira G, De Maria R, Larocca LM and Pallini R. Expression of EGFRvIII in glioblastoma: prognostic significance revisited. Neoplasia 2011; 13: 1113-1121.
[31] Brandes AA, Franceschi E, Tosoni A, Blatt V, Pession A, Tallini G, Bertorelle R, Bartolini S, Calbucci F, Andreoli A, Frezza G, Leonardi M, Spagnolli F and Ermani M. MGMT promoter methylation status can predict the incidence and outcome of pseudoprogression after concomitant radiochemotherapy in newly diagnosed glioblastoma patients. J Clin Oncol 2008; 26: 2192-2197.
[32] Kong DS, Song SY, Kim DH, Joo KM, Yoo JS, Koh JS, Dong SM, Suh YL, Lee JI, Park K, Kim JH and Nam DH. Prognostic significance of c-Met expression in glioblastomas. Cancer 2009; 115: 140-148.